NRSCC

esa

ESA–MOST Dragon Cooperation

中国科技部-欧洲空间局“龙计划”合作

2017 DRAGON 4 SYMPOSIUM

2017年“龙计划”四期学术研讨会

26–30 June 2017 | Copenhagen, Denmark

2017年6月26-30日，丹麦 哥本哈根

INCIDENCE ANGLE NORMALIZATION OF SENTINEL-1 WIDE AND EXTRA WIDE SWATH DATA FOR OCEANIC APPLICATIONS

Dr. Konstantinos Topouzelis

Marine Remote Sensing Group
Department of Marine Sciences
University of the Aegean

Oil spill detection

Photo-interpretation

Semi-automatic detection

Fully automatic detection

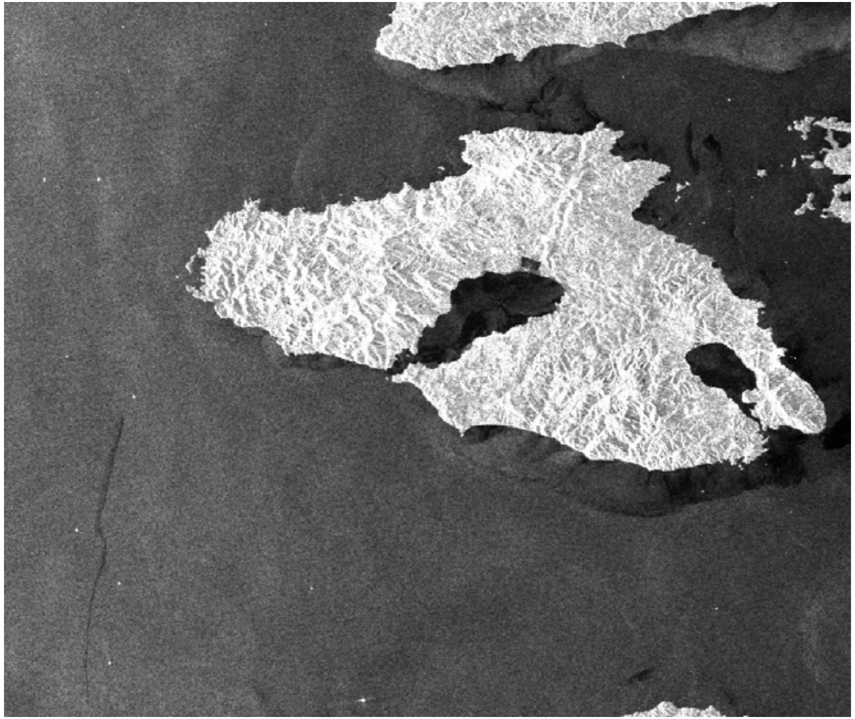

Oil spill detection

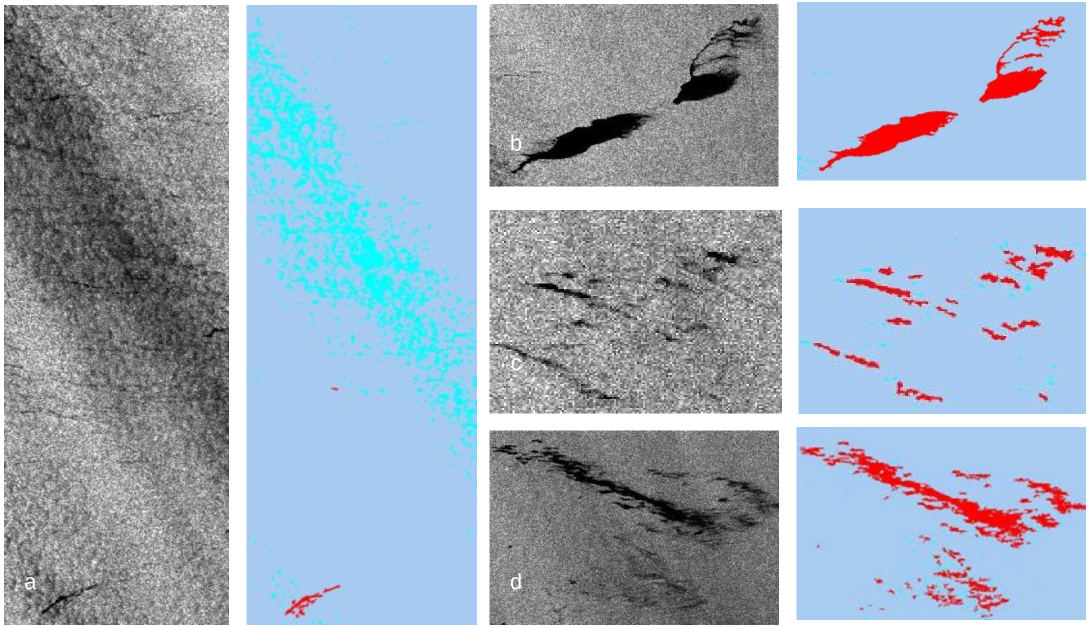

Example of automatic oil spill detection

Oil spill detection

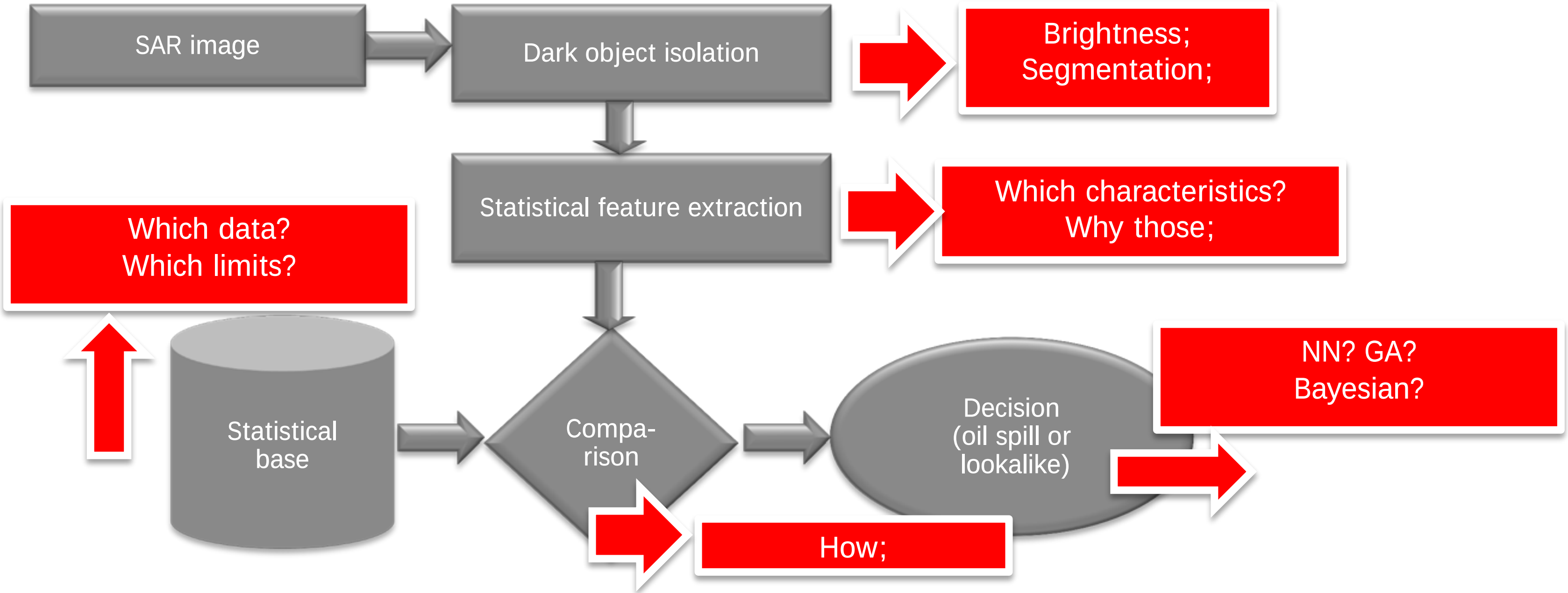

Topouzelis, K., Psyllos,A. 2012, Oil spill feature selection and classification using decision tree forest on SAR image data. ISPRS, J. Photogram. Remote Sensing, 68, pp. 135–143

SAR oceanic phenomena

Oceanic phenomena	Atmospheric phenomena
Channel plumes	Atmospheric gravity waves
Coastal discharges	Atmospheric convective cells
Coastal fronts	Atmospheric boundary layer rolls
Coastal rivers	Katabatic winds
Ocean currents	Land/sea breeze
Current fronts	Atmospheric fronts
Estuaries	Island wakes
Intertidal zone	Coastal winds
Oceanic eddies	Rain events
Oceanic internal waves	
Oceanic wakes	
Oil pollution	
Ship wakes	
Underwater bottom topography	
Upwelling	

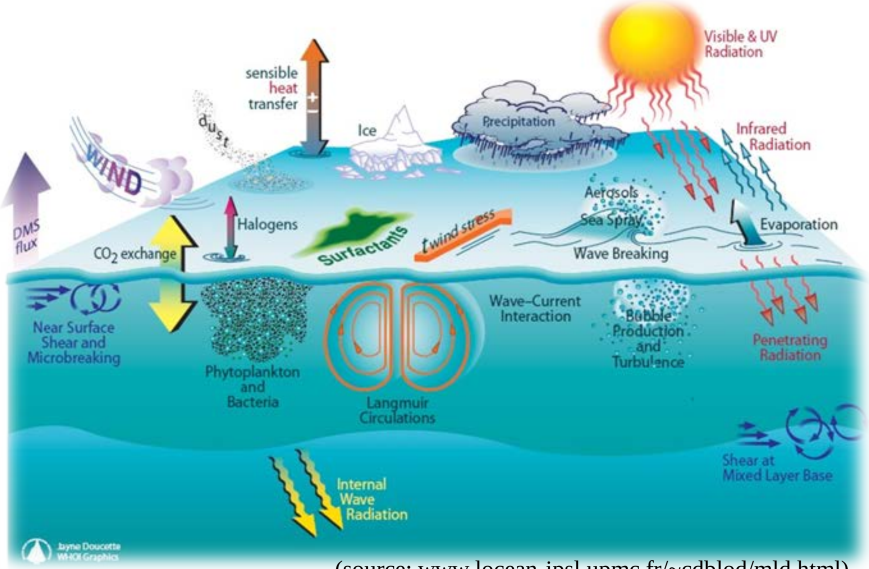

(source: www.locean-ipsl.upmc.fr/~cdblod/mld.html)

Topouzelis K. and Kitsiou D., Detection and classification of mesoscale atmospheric, phenomena above sea in SAR imagery, Remote Sensing of Environment, 160, 2015

SAR oceanic phenomena

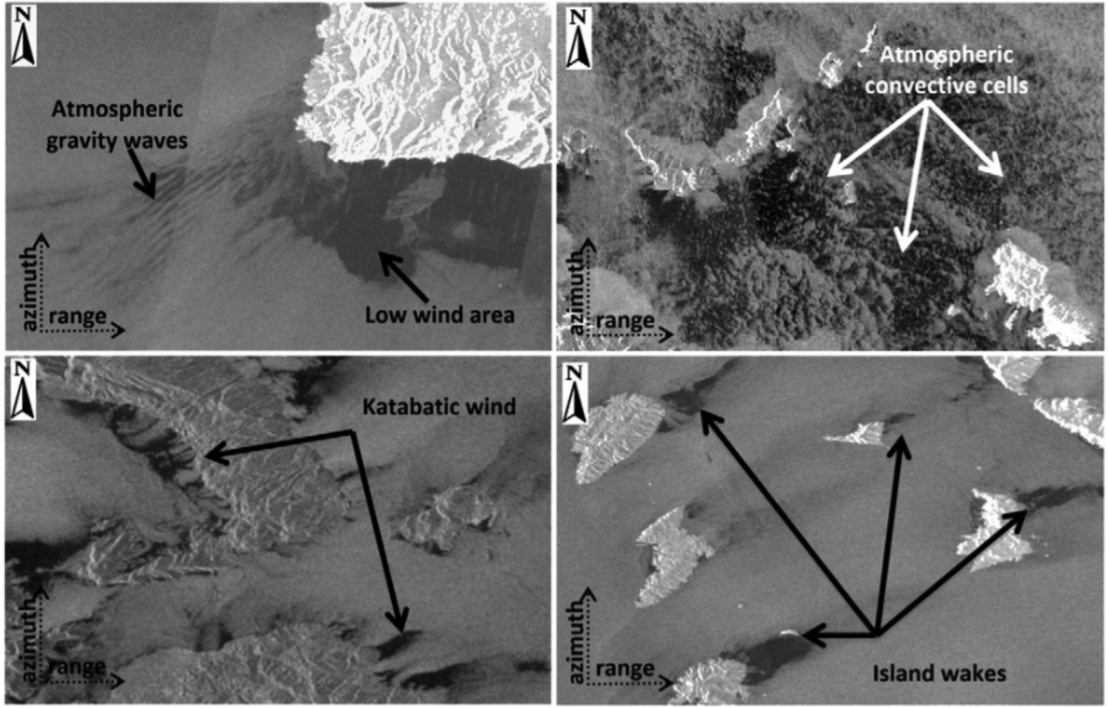

Topouzelis K. and Kitsiou D., Detection and classification of mesoscale atmospheric, phenomena above sea in SAR imagery, Remote Sensing of Environment, 160, 2015

SAR Normalization

Satellite image

Calibration

Land marking - Re-projection

Incidence Angle Normalization

Dark area detection

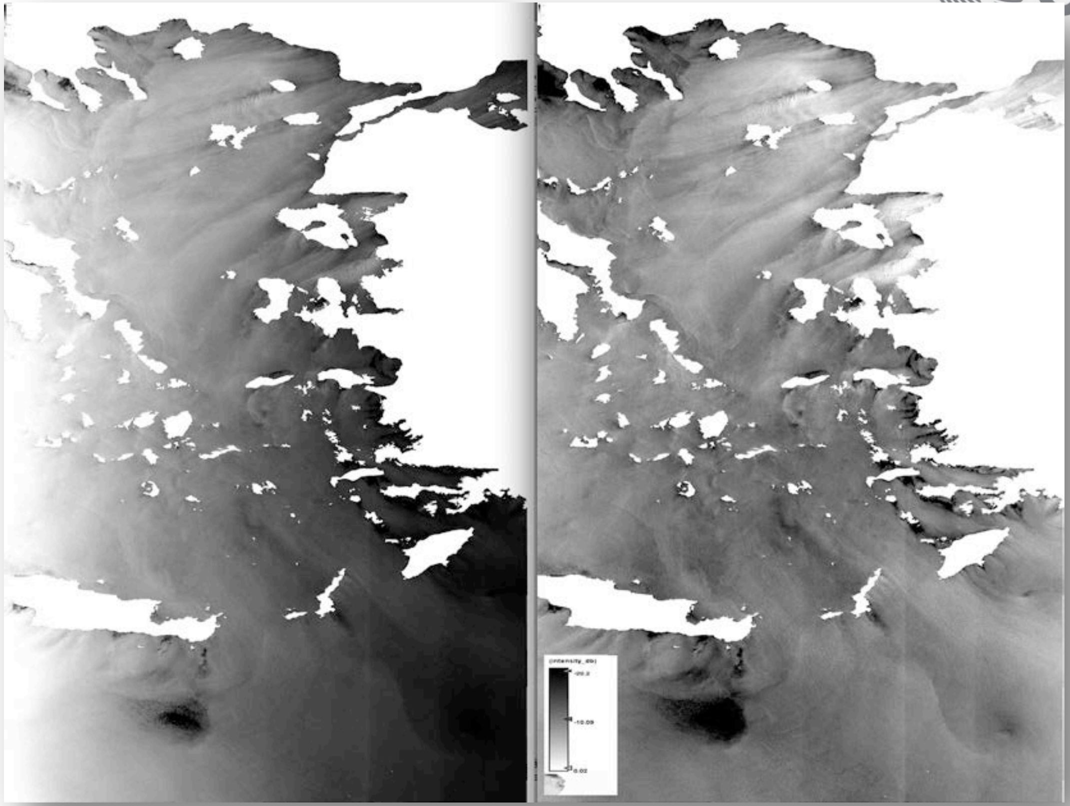

Topouzelis, K. and Kitsiou, 2014, D. Sea State Primitive Object Creation from SAR Data, International Journal of Geosciences, 5, 1561-1570

Incidence angle normalization

3 WAYS:

1. Square cosine correction

$$\sigma^0_{ref} = \frac{\sigma^0_\theta \cos^2(\theta_{ref})}{\cos^2(\theta)}$$

2. Theoretical backscattering shape function derivation

3. Empirical range fit

Topouzelis, K., Singha, S., Kitsiou, D., 2016. Incidence angle normalization of Wide Swath SAR data for oceanographic applications. Open Geosci. 8. doi:10.1515/geo-2016-0029

Incidence angle normalization

theoretical backscattering shape function derivation

Uses only information from the image geometry: its incident angle θ and the theoretical NRCS value at wind speed of 2.5-3m/sec

For C band SAR (ENVISAT-WSM) NRCS at incidence angles 16°-45° follow a linear distribution among 2.5-(-20)dB.

the theoretical $NRCS_{\theta}$ (or σ^{0}_{θ}) values for θ 16°-45° is described

$$\sigma^{0}_{\theta} = -0.776\,\theta + 14.914$$

For reference angle (θ=30°) the symmetric function $(\sigma^{0}_{\theta})^{-1}$ is:

$$(\sigma^{0}_{\theta(30°)})^{-1} = 0.776\,\theta - 31.638$$

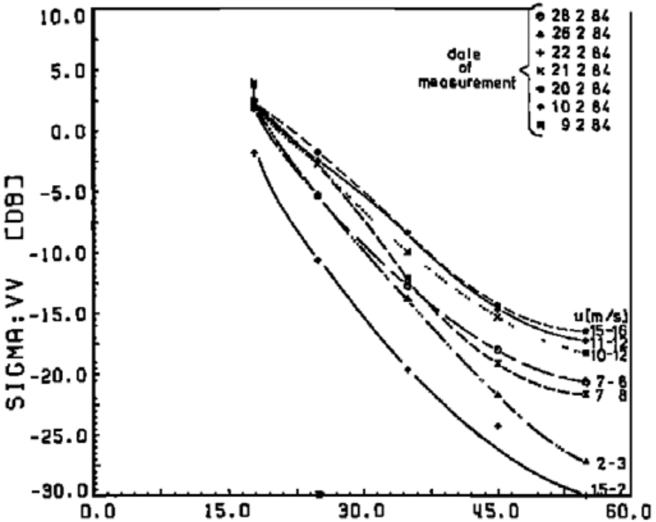

Feindt, F., Wismann, V., Alpers, W., Keller, W.C., 1986. Airborne measurements of the ocean radar cross section at 5.3 GHz as a function of wind speed. Radio Sci. 21, 845–856. doi:10.1029/RS021i005p00845

Topouzelis, K., Singha, S., Kitsiou, D., 2016. Incidence angle normalization of Wide Swath SAR data for oceanographic applications. Open Geosci. 8. doi:10.1515/geo-2016-0029

SAR Normalization

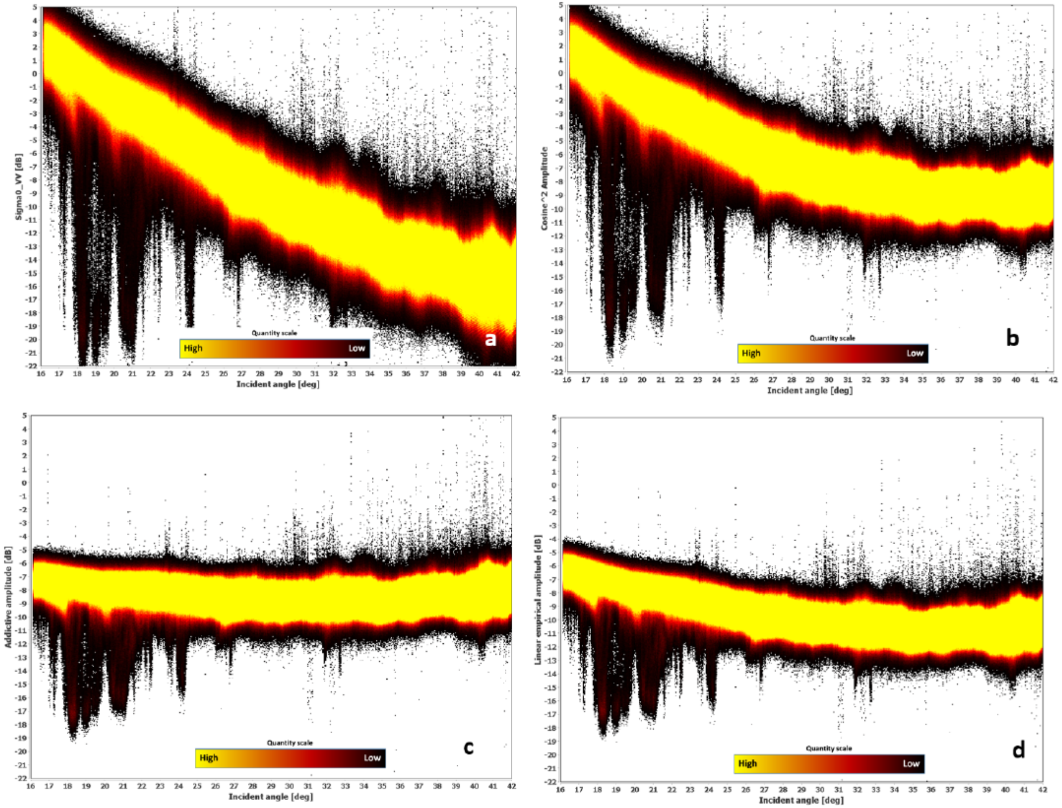

Figure 4: Range profile plots from Figure 3 images: (a) L1B ASAR WSM product, (b) Squared cosine normalization, (c) Theoretical normalization, (d) Linear empirical normalization.

Topouzelis, K., Singha, S., Kitsiou, D., 2016. Incidence angle normalization of Wide Swath SAR data for oceanographic applications. Open Geosci. 8. doi:10.1515/geo-2016-0029

SAR Normalization

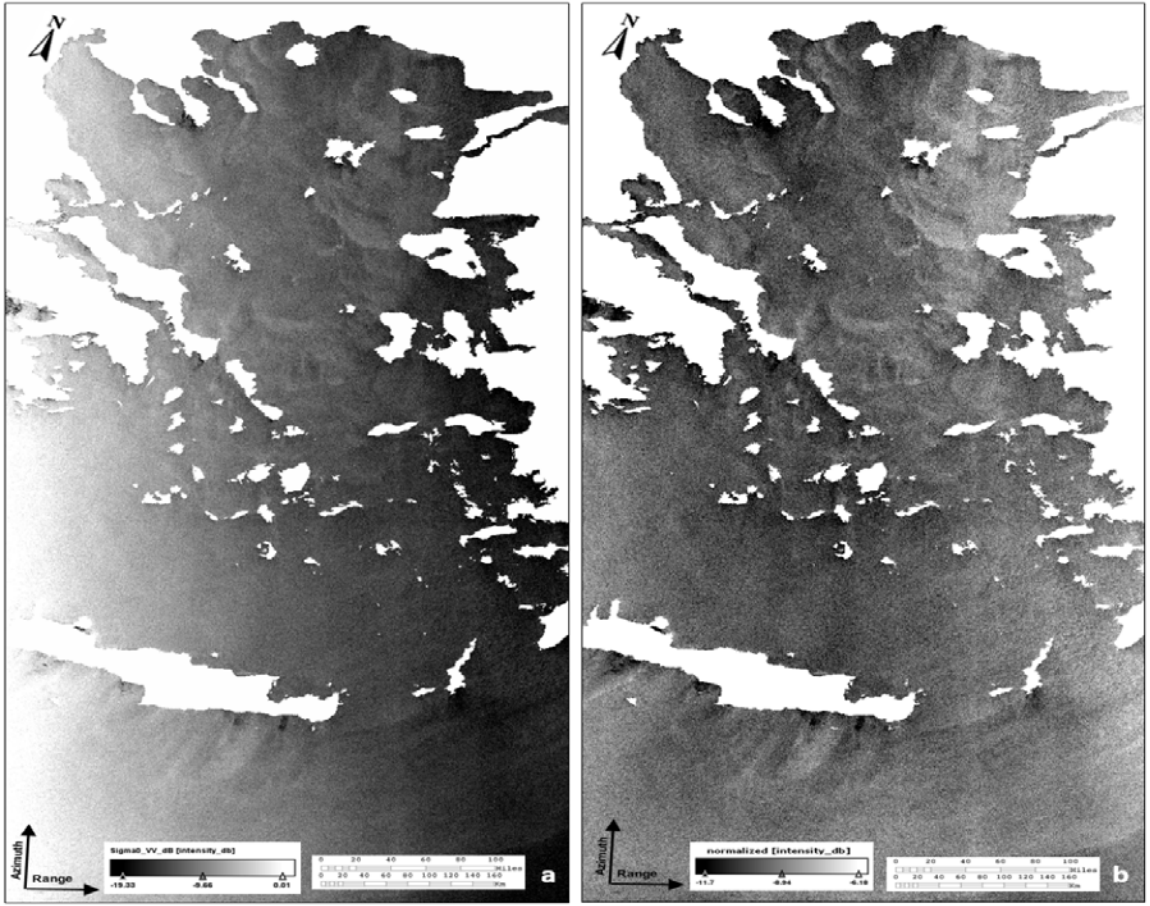

Topouzelis, K., Singha, S., Kitsiou, D., 2016. Incidence angle normalization of Wide Swath SAR data for oceanographic applications. Open Geosci. 8. doi:10.1515/geo-2016-0029

Dark area detection

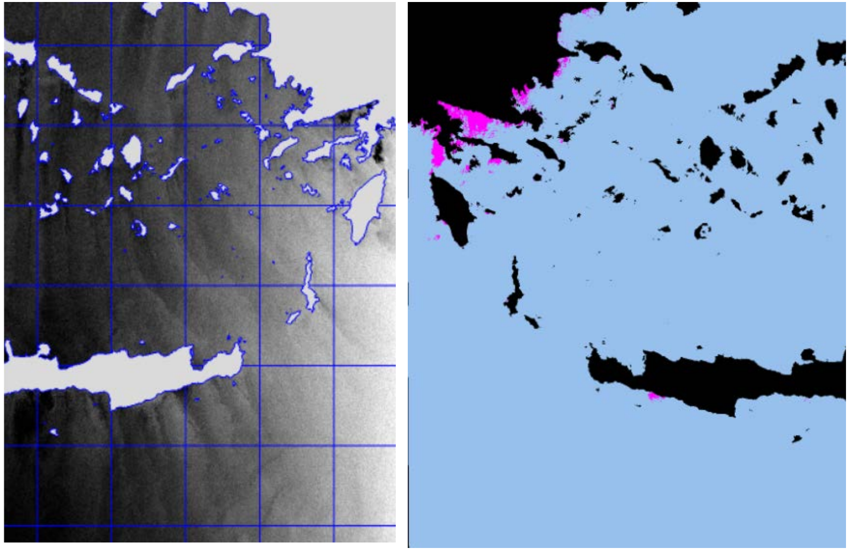

Three thresholds for dark area detection:

Global Threshold (GT): $Mean_{image} - St.Dev_{image}$

Local Threshold 1(LT1): $Mean_{pixel} - Mean_{subarea}$

Local Threshold 2(LT2): $Mean_{pixel} - (Mean_{subarea} - St.Dev_{subarea})$

ENVISAT WSM

Year **2011**

10 ENVISAT ASAR IMAGES

Wide Swath (WS)

Resolution: 75m x 75m

Polarization: VV

Area Cover: Aegean Sea

Several oceanographic phenomena present

Comparison Masks

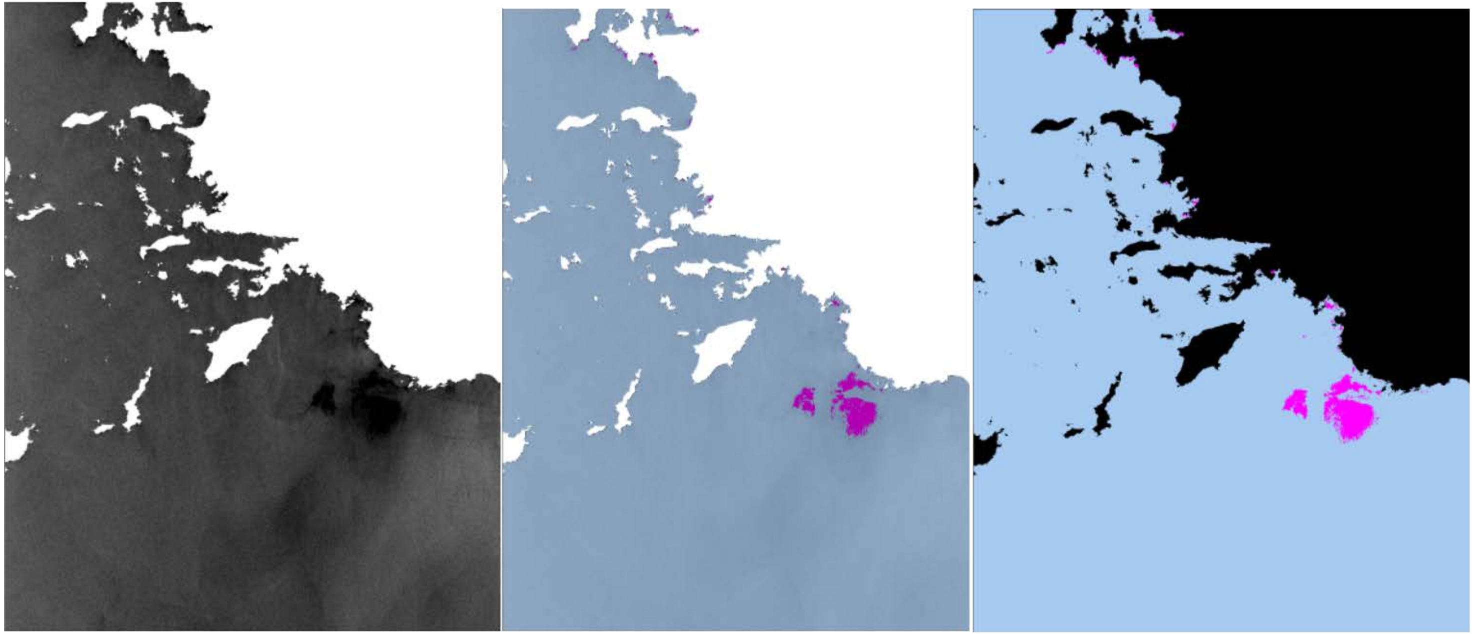

Results

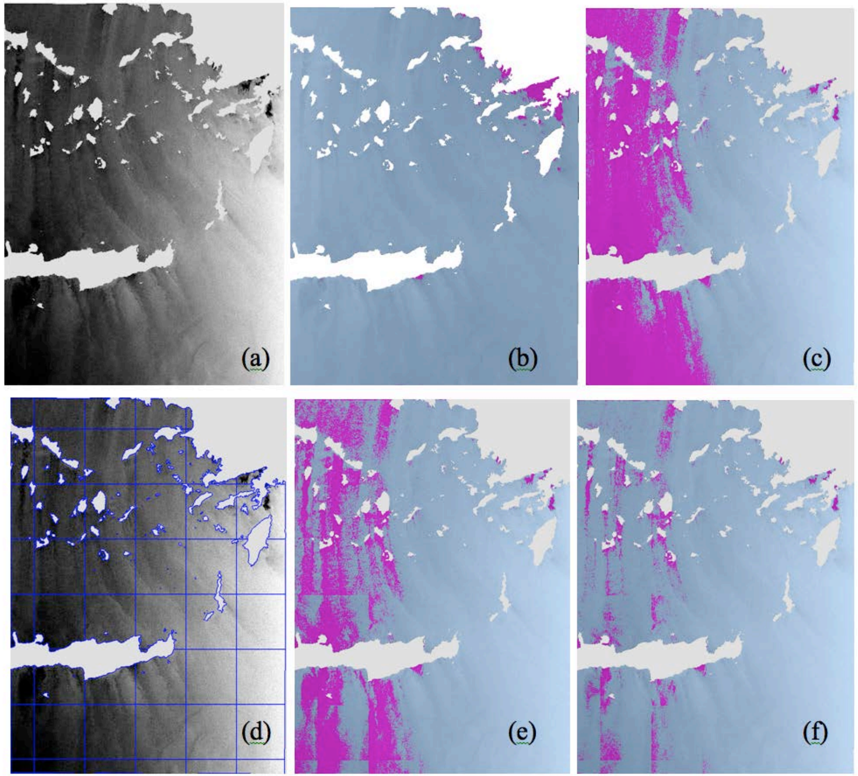

a) Original image,

b) Detection in the normalized image

c) Detection in original image by global threshold

d) Sub areas for local thresholds calculation

e) Detection in original image by LT1

f) Detection in original image by LT2.

Results -Comparison matrix

	Normalized image (global threshold)			Original (Local threshold 2)		
User \ Reference Class	Dark area	Background	Sum	Dark area	Background	Sum
Dark area	274992	43473	318465	43418	1299337	1342755
Background	0	31256041	31256041	32840	30198911	30231751
Sum	274992	31299514		76258	31498248	
Producer acc.	1	0.998		0.569	0.958	
User acc.	0.863	1		0.032	0.999	
KIA Per Class	1	0.862		0.550	0.030	
Overall Accuracy	0.998			0.958		
KIA	0.926			0.057		

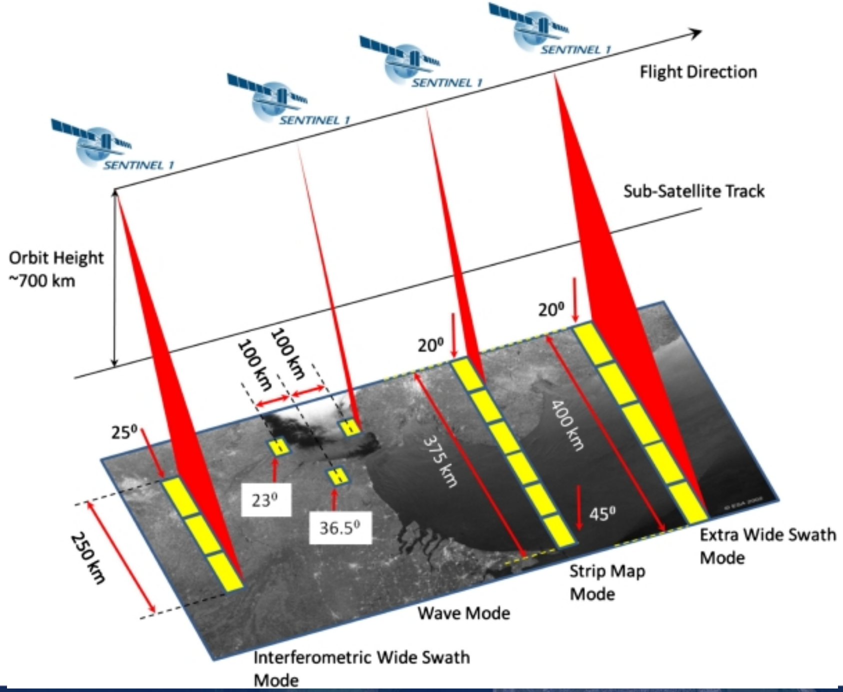

https://sentinel.esa.int/web/sentinel/user-guides/sentinel-1-sar/acquisition-modes

SENTINEL-1 INTERFEROMETRIC WIDE SWATH MODE

Characteristic	Value
Swath width	250 km
Incidence angle range	29.1° - 46.0°
Sub-swaths	3
Azmiuth steering angle	± 0.6°
Azmiuth and range looks	Single
Polarisation options	Dual HH+HV, VV+VH Single HH, VV
Maximum Noise Equivalent Sigma Zero (NESZ)	-22 dB
Radiometric stability	0.5 dB (3σ)
Radiometric accuracy	1 dB (3σ)
Phase error	5°

Table 1: Characteristics of Interferometric Wide swath mode

The table below shows the incidence and off-nadir angles for Interferometric Wide swath mode beams.

Beam	IW1	IW2	IW3
Off-nadir angles at min orbit altitude	27.53-32.48	32.38-36.96	36.87-40.40
Incidence angles at min orbit altitude	30.86-36.59	36.47-41.85	41.75-46.00
Off-nadir angles at max orbit altitude	26.00-30.96	30.86-35.43	35.35-38.88
Incidence angles at max orbit altitude	29.16-34.89	34.77-40.15	40.04-44.28

Table 2: Angles for Interferometric Wide swath mode beams

https://sentinel.esa.int/web/sentinel/user-guides/sentinel-1-sar/acquisition-modes/extra-wide-swath

24.04.2015

S1A_IW_GRDH_1SDV_20150424T063905_20150424T063934_005622_00733B_534A

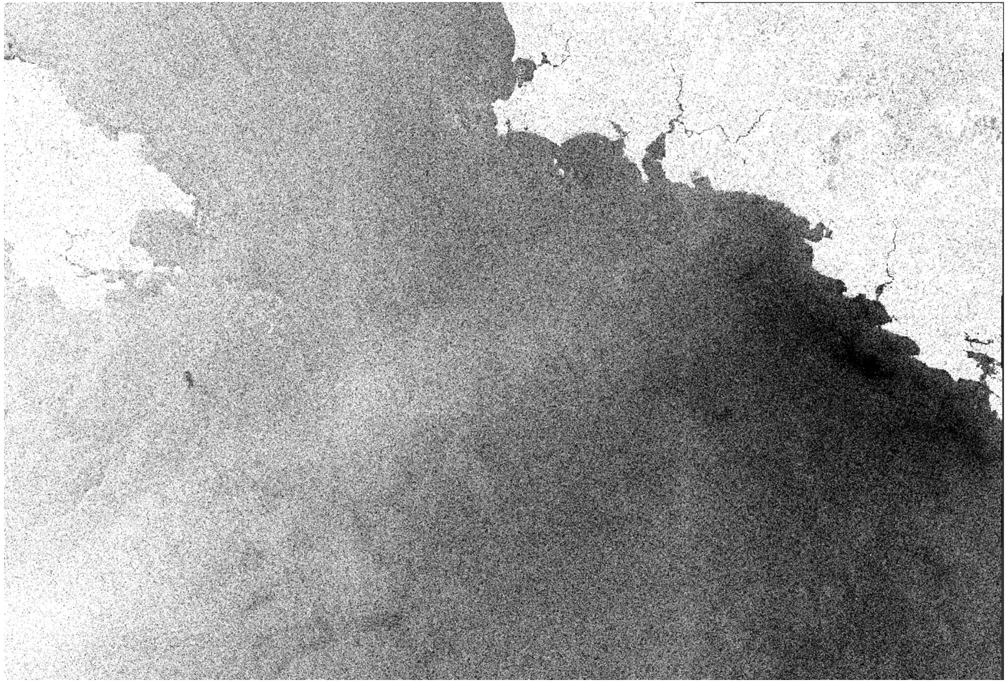

26.04.2015

S1A_IW_GRDH_1SDV_20150426T154823_20150426T154848_005657_007411_DD88

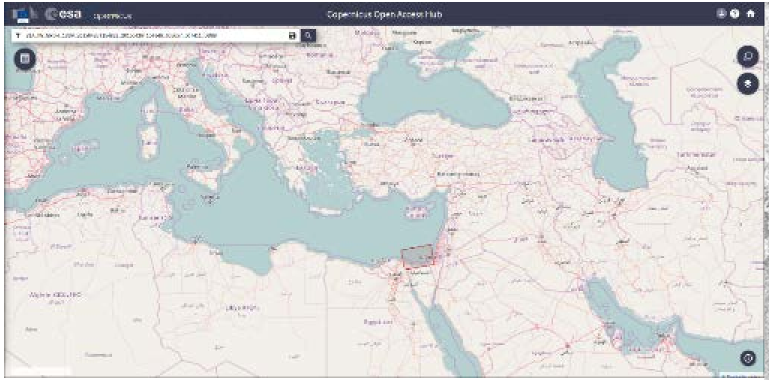

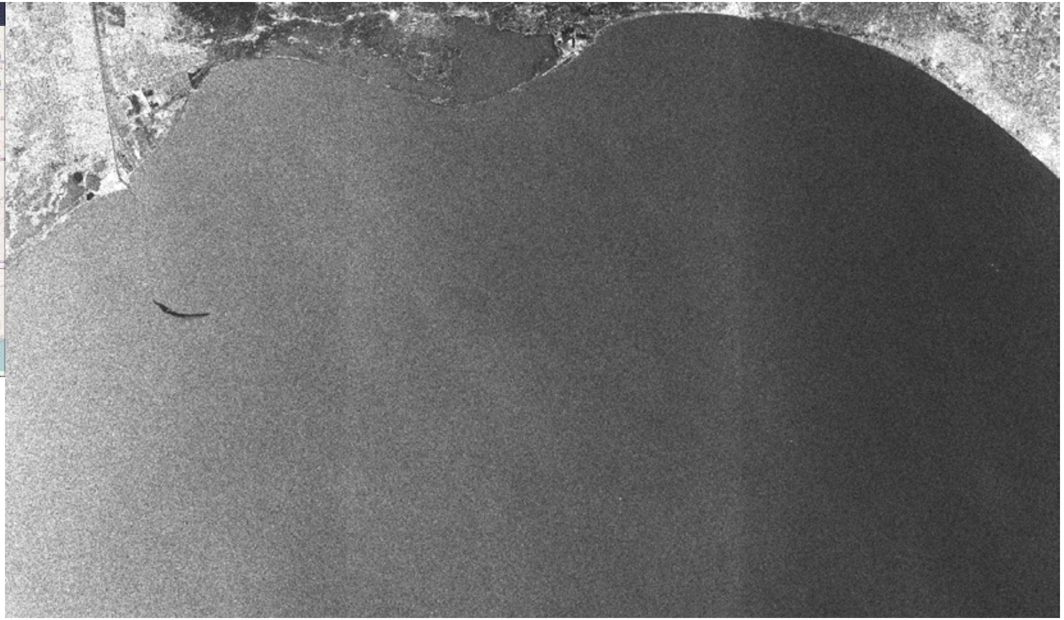

26.04.2015

S1A_IW_GRDH_1SDV_20150426T155118_20150426T155143_005657_007411_C1E5

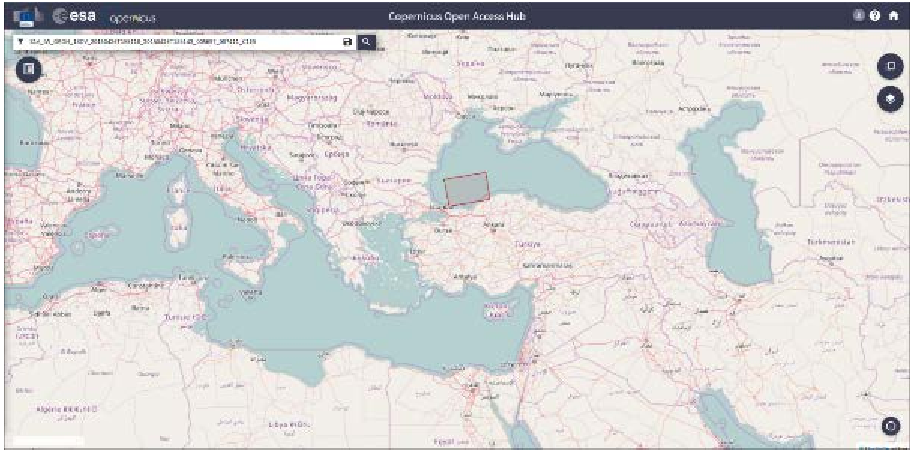

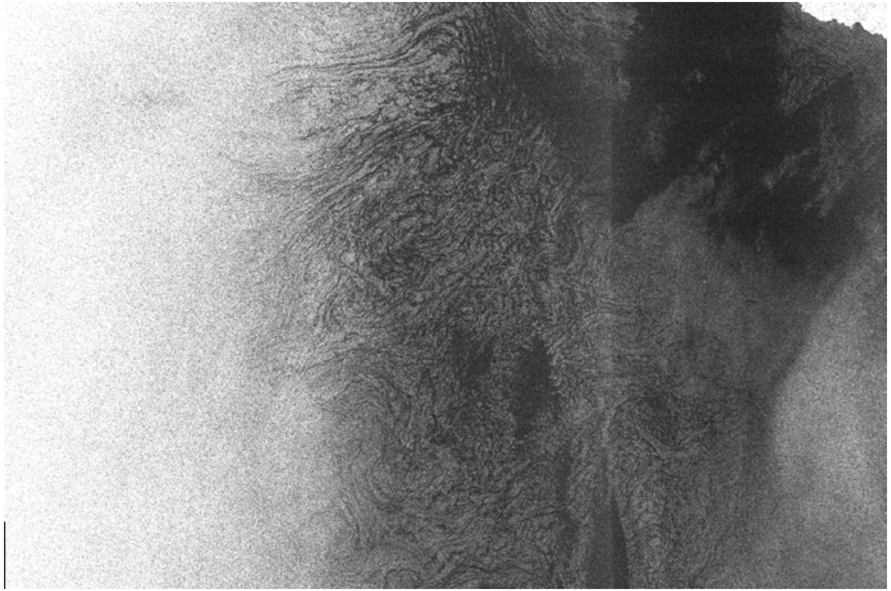

01.05.2015

S1A_IW_GRDH_1SDV_20150501T045633_20150501T045647_005723_00758B_008D

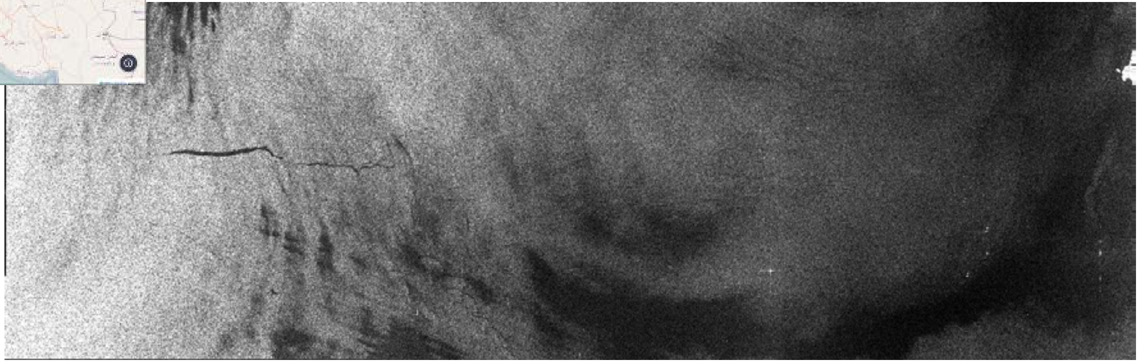

Incidence angle normalization

theoretical backscattering shape function derivation

Uses only information from the image geometry: its incident angle θ and the theoretical NRCS value at wind speed of 2.5-3m/sec.

For C band SAR (**S1 WI**) NRCS at incidence angles 29.1°- 46° follow a linear distribution among -10 dB to -21.5dB.

the theoretical $NRCS_{\theta}$ (or σ^0_{θ}) values for θ 29 °-46° is described

$$\sigma^0_{\theta} = -0.68\,\theta + 9.80$$

For reference angle (θ=37,5°) the symmetric function $(\sigma^0_{\theta})^{-1}$ is:

$$(\sigma^0_{\theta(30°)})^{-1} = 0.68\,\theta - 41.30$$

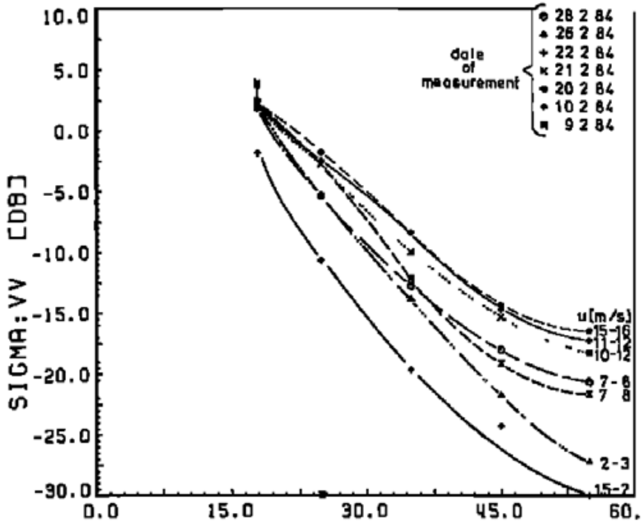

Feindt, F., Wismann, V., Alpers, W., Keller, W.C., 1986. Airborne measurements of the ocean radar cross section at 5.3 GHz as a function of wind speed. Radio Sci. 21, 845–856. doi:10.1029/RS021i005p00845

S1A_IW_GRDH_1SDV_20170623T042254_20170623T042319_017156_01C9B0_2AF9

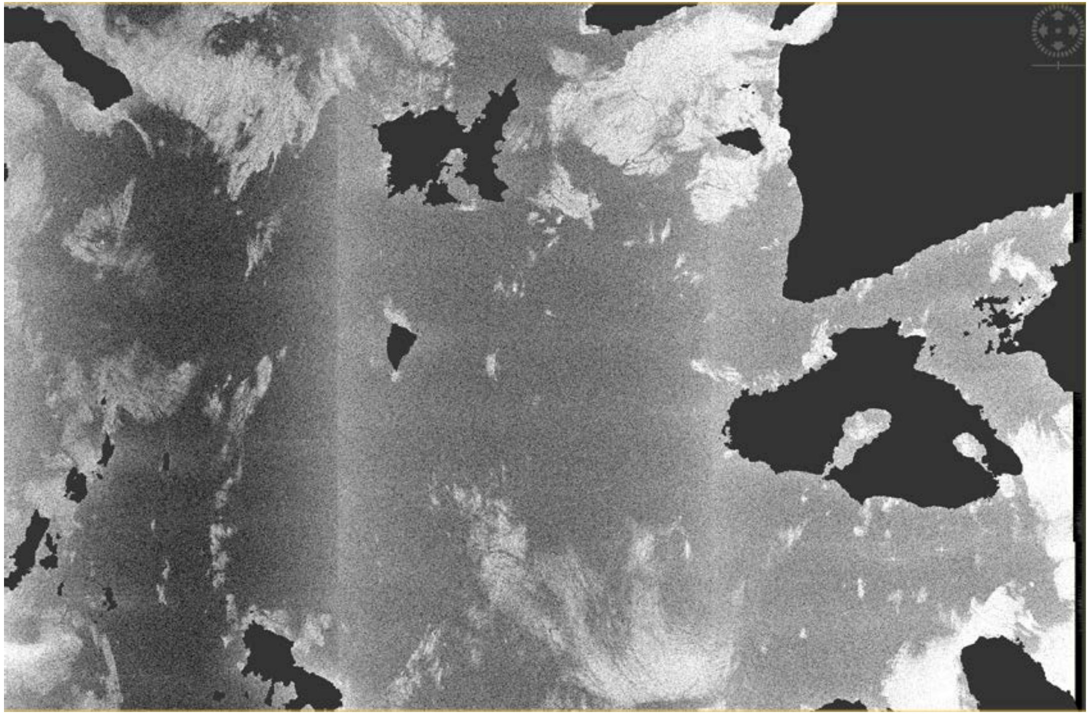

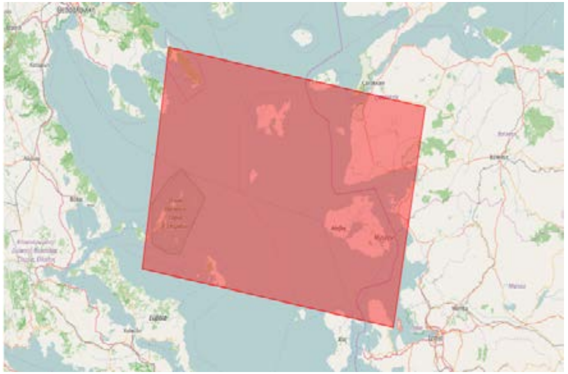

S1A_IW_GRDH_1SDV_20170623T042254_20170623T042319_017156_01C9B0_2AF9

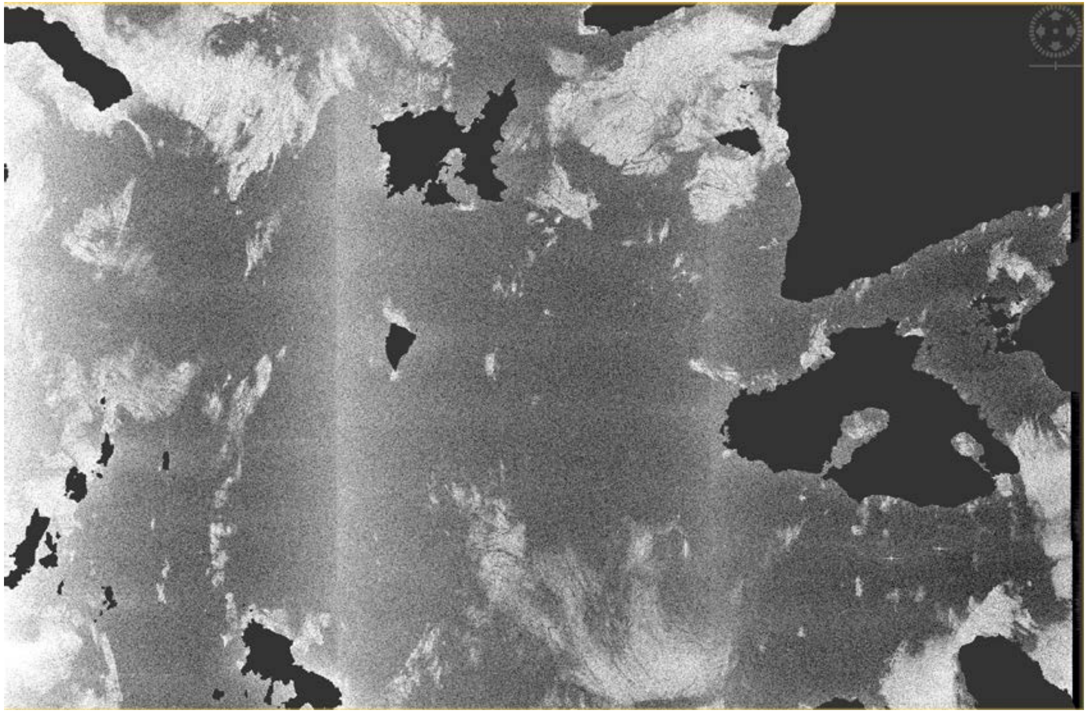

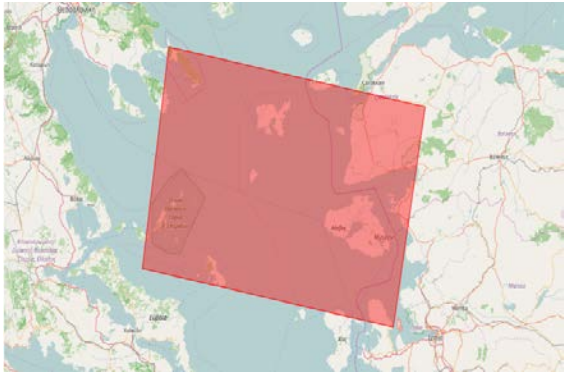

Low wind areas

S1B_IW_GRDH_1SDV_20170623T161436_20170623T161501_006180_00ADB3_F6AD

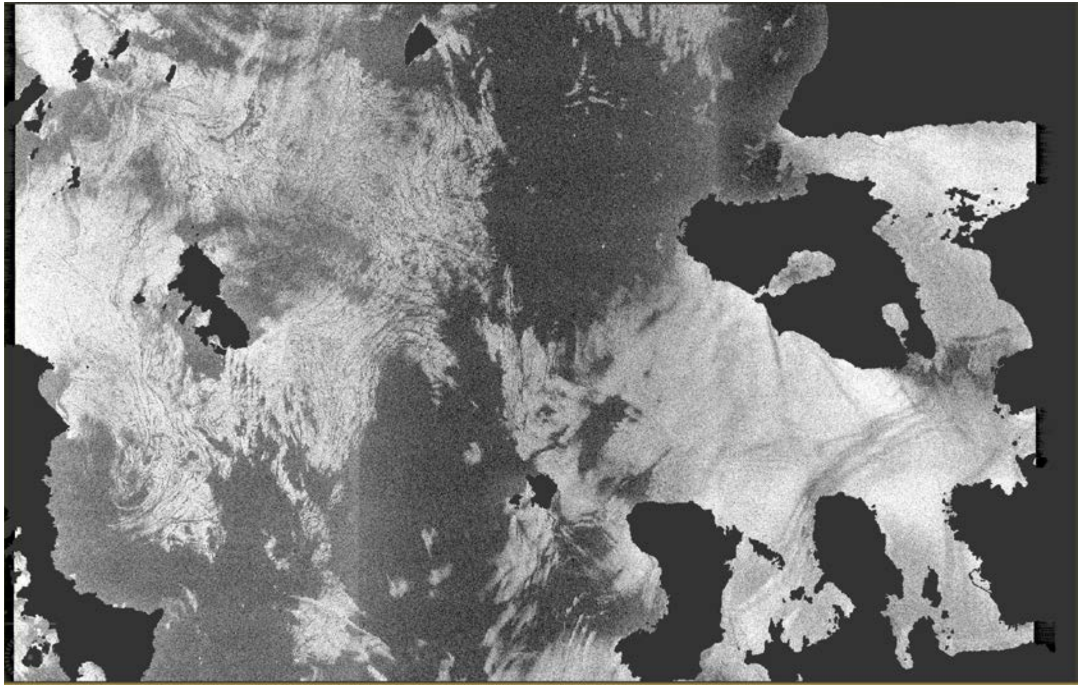

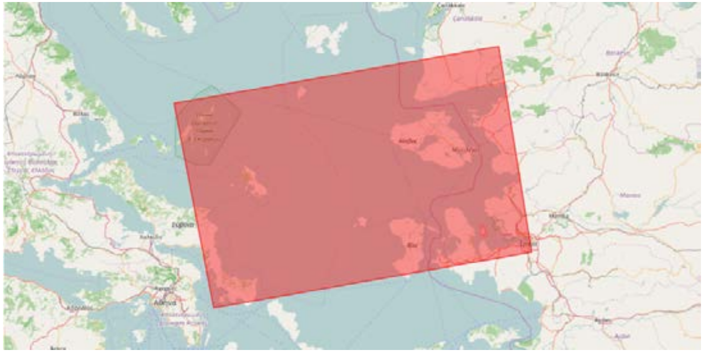

S1B_IW_GRDH_1SDV_20170623T161436_20170623T161501_006180_00ADB3_F6AD

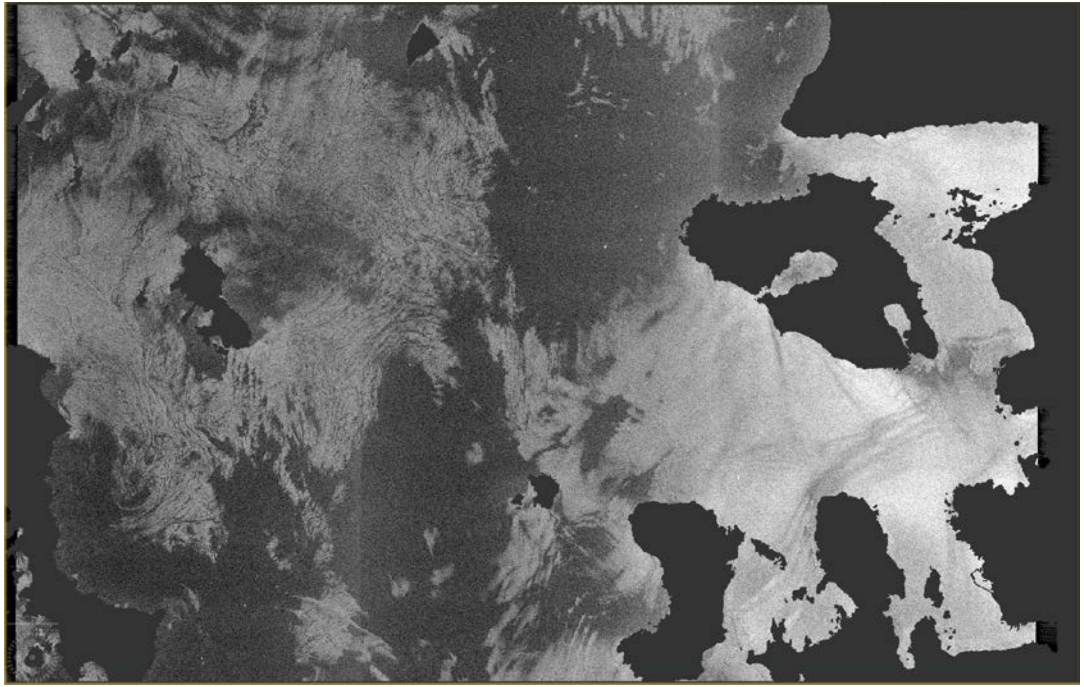

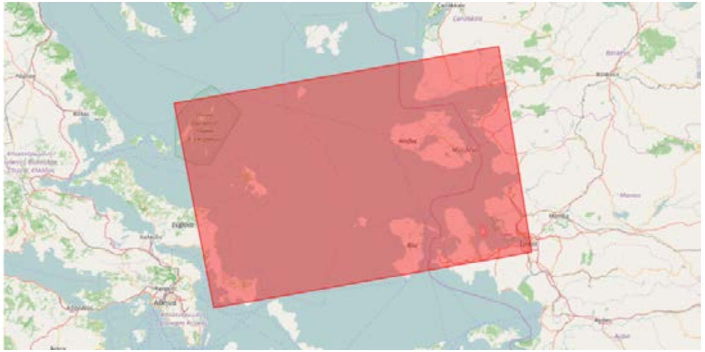

Low wind areas

S1A_IW_GRDH_1SDV_20170623T042434_20170623T042459_017156_01C9B0_4F92

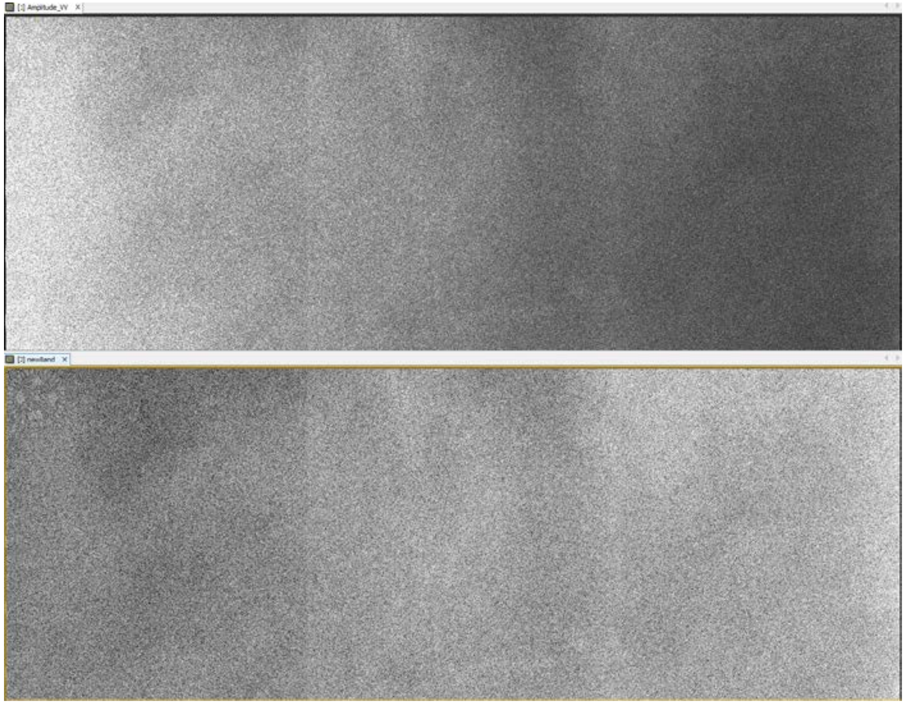

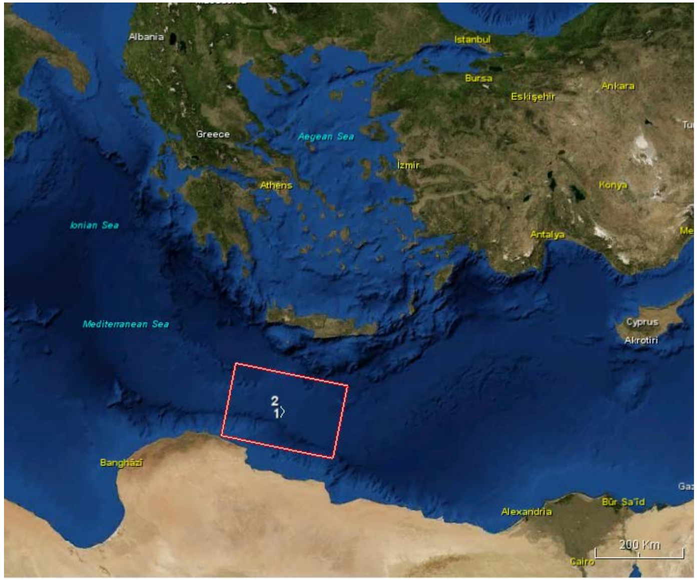

S1A_IW_GRDH_1SDV_20170623T042434_20170623T042459_017156_01C9B0_4F92

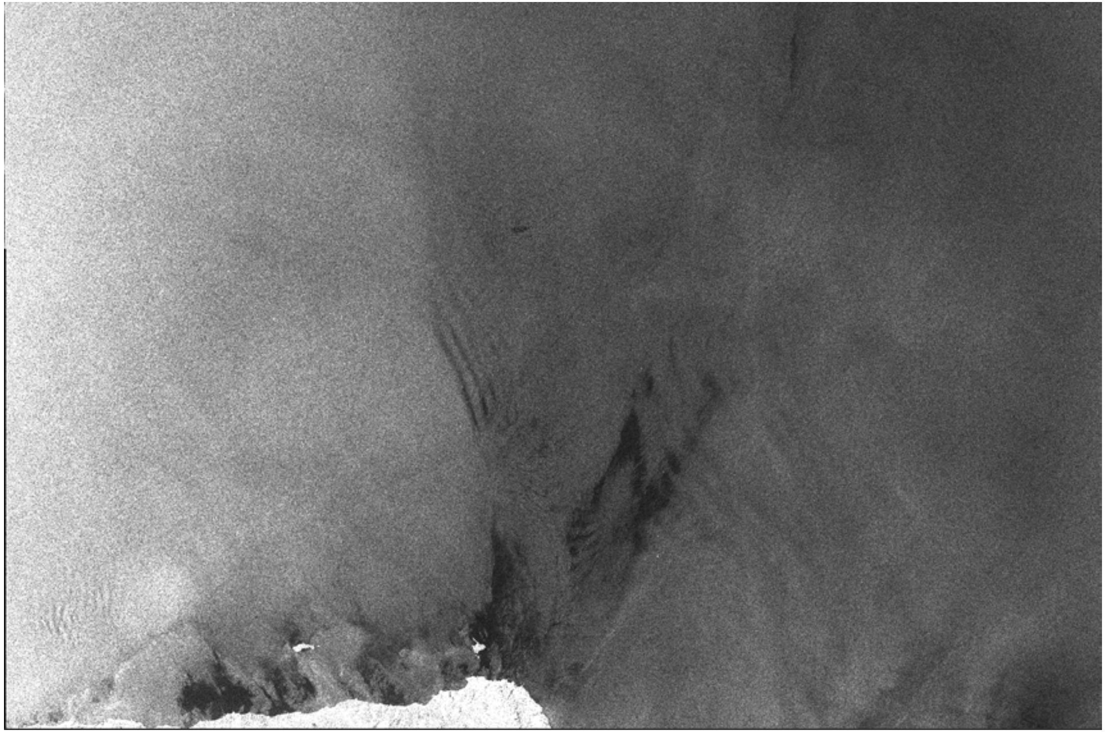

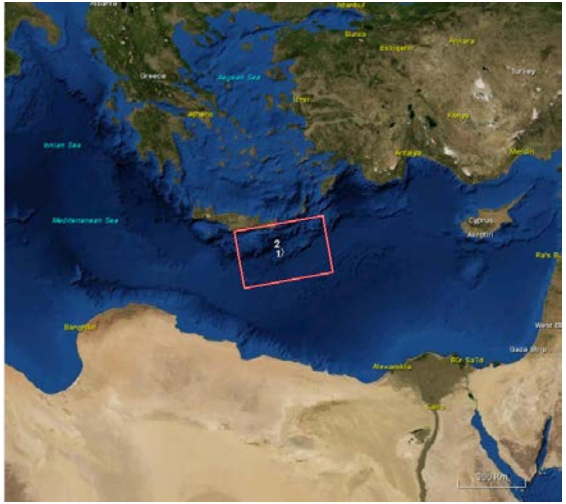

medium wind areas

S1A_IW_GRDH_1SDV_20170623T042434_20170623T042459_017156_01C9B0_4F92

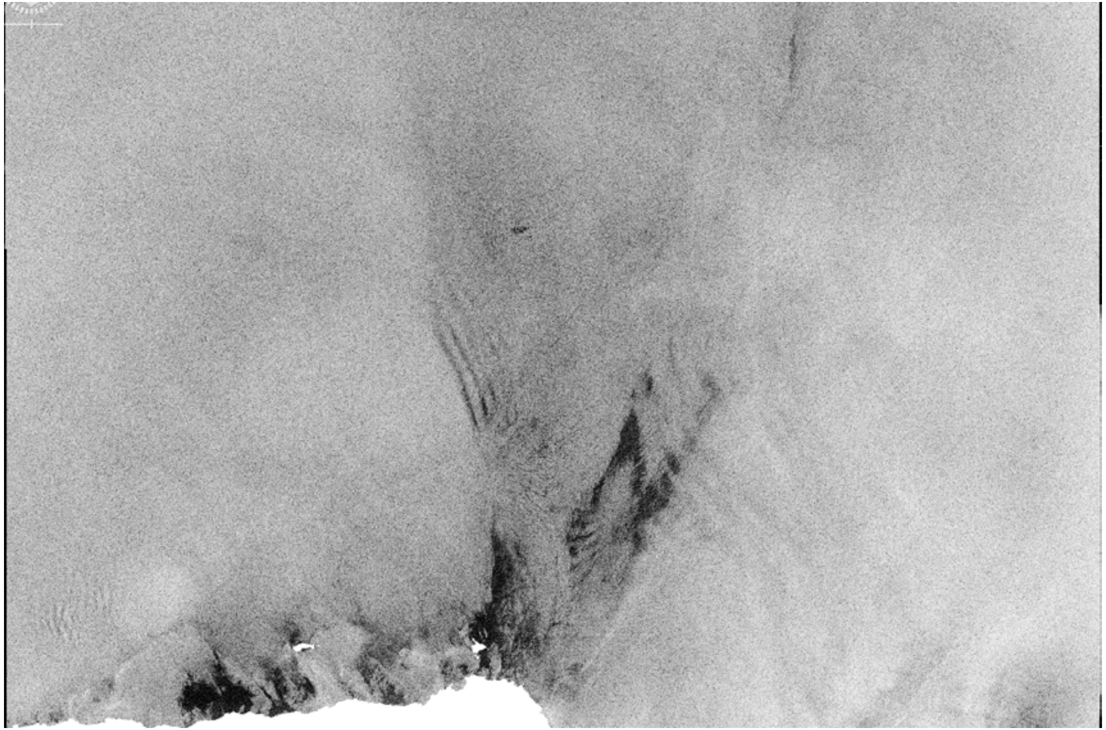

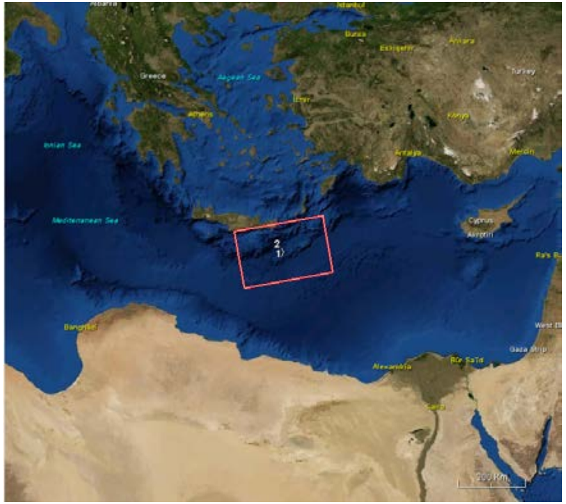

medium wind areas

S1B_IW_GRDH_1SDV_20170624T041531_20170624T041556_006187_00ADED_0993

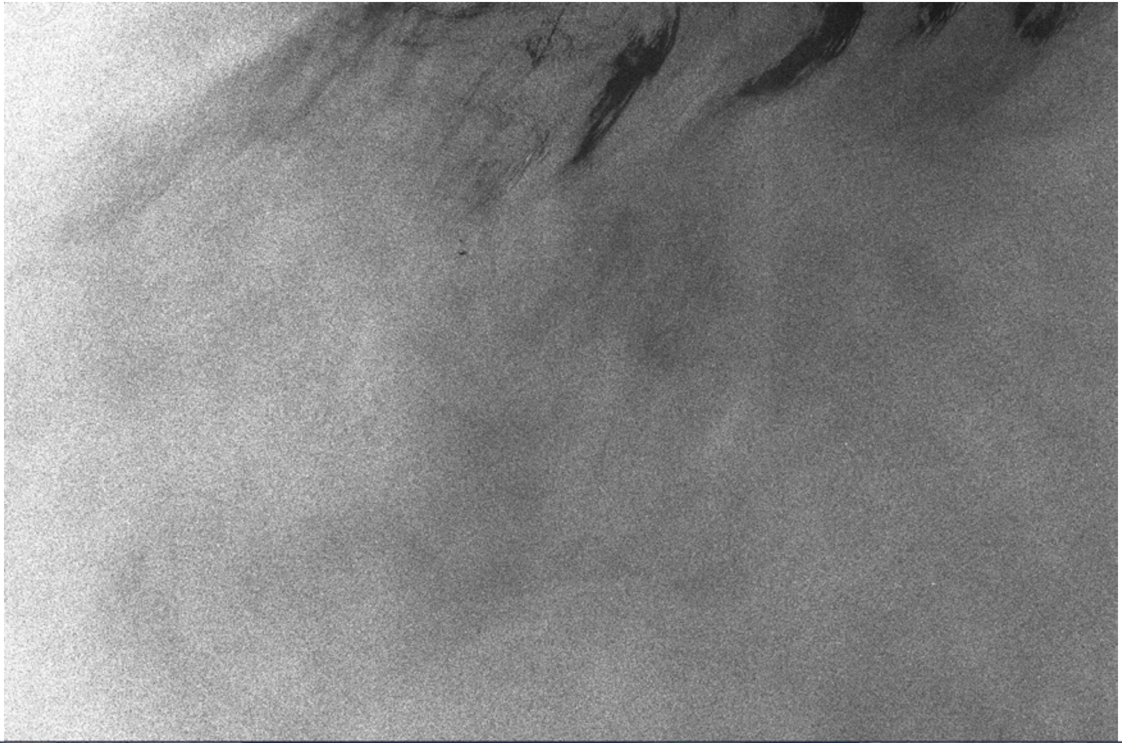

S1B_IW_GRDH_1SDV_20170624T041531_20170624T041556_006187_00ADED_0993

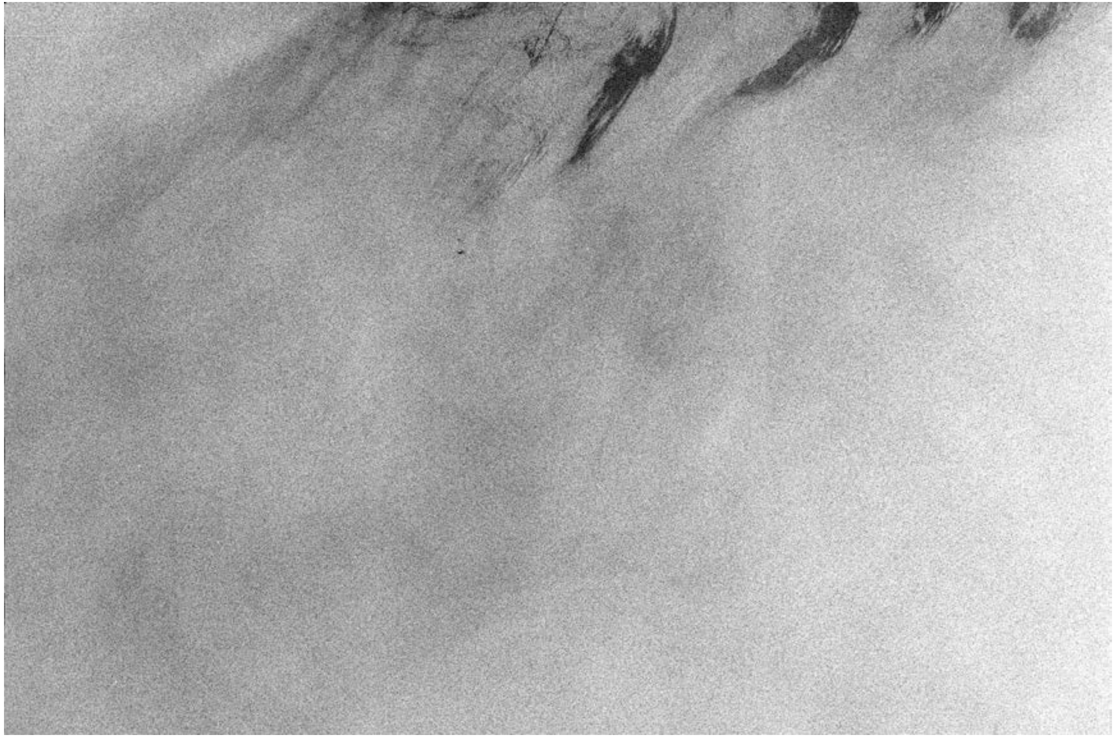

Conclusions

Increased stability for the dark detection after normalization

Normalization increased the ability to detect dark areas

Local thresholds found insufficient for dark area detection

Important procedure for operational procedures (oil spills, low wind areas)

Marine Remote Sensing Group (MRSG)

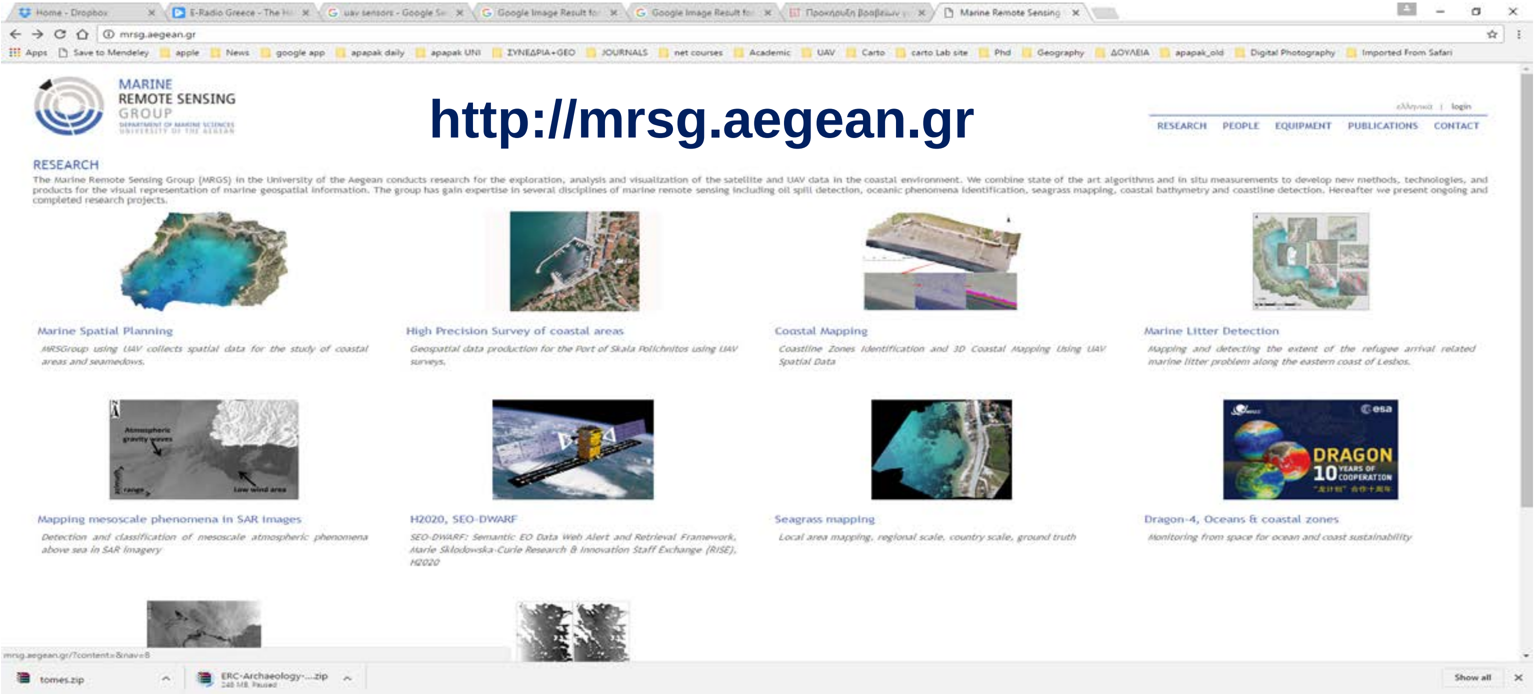

http://mrsg.aegean.gr

MARINE
REMOTE SENSING
GROUP
DEPARTMENT OF MARINE SCIENCES
UNIVERSITY OF THE AEGEAN
http://mrsg.aegean.gr

Dr. Konstantinos Topouzelis

topouzelis@marine.aegean.gr